Pressure-induced enhancement of superfluid density in transition metal dichalcogenides with and without charge density wave

Islam, S. S.; Sazgari, V.; Witteveen, Catherine; Graham, J. N.; Gerguri, O.; Král, P.; Bartkowiak, M.; Luetkens, H.; Khasanov, R.; von Rohr, Fabian; Guguchia, Z.

How to cite

ISLAM, S. S. et al. Pressure-induced enhancement of superfluid density in transition metal dichalcogenides with and without charge density wave. In: Physical review research, 2025, vol. 7, n° 1, p. 013324. doi: 10.1103/PhysRevResearch.7.013324

This publication URL: https://archive-ouverte.unige.ch/unige:186432
Publication DOI: 10.1103/PhysRevResearch.7.013324

Pressure-induced enhancement of superfluid density in transition metal dichalcogenides with and without charge density wave

S. S. Islam [1,*] V. Sazgari [1,*] C. Witteveen [2,3,*] J. N. Graham [1] O. Gerguri,[1,3] P. Král,[1] M. Bartkowiak,[1] H. Luetkens,[1] R. Khasanov [1] F. O. von Rohr,[2,†] and Z. Guguchia [1,‡]

[1]*PSI Center for Neutron and Muon Sciences CNM, 5232 Villigen PSI, Switzerland*

[2]*Department of Quantum Matter Physics, University of Geneva, CH-1211 Geneva, Switzerland*

[3]*Department of Physics, University of Zurich, Winterthurerstrasse 190, 8057 Zurich, Switzerland*

(Received 11 June 2024; revised 21 December 2024; accepted 5 March 2025; published 28 March 2025)

Gaining a deeper understanding of the interplay between charge density wave (CDW) order and superconductivity in transition metal dichalcogenides (TMDs), particularly within the (4H/2H)-NbX_2 (X = Se and S) family, remains an open and intriguing challenge. A systematic microscopic study across various compounds in this family is therefore required to unravel this complex interplay. Here, we report on muon spin rotation (μSR) and magnetotransport experiments investigating the effects of hydrostatic pressure on the superconducting transition temperature (T_c), the temperature-dependent magnetic penetration depth (λ_{eff}), and the charge density wave order (CDW) in two layered chalcogenide superconductors: 4H-$NbSe_2$, which exhibits CDW order, and 2H-NbS_2, which lacks such order. Our observations reveal a substantial 75% enhancement of the superfluid density (n_s/m^*) in 4H-$NbSe_2$ upon the maximum applied pressure of ∼2 GPa, surpassing that of 2H-$NbSe_2$. Despite the absence of CDW order, a sizable 20% growth in superfluid density is also observed for 2H-NbS_2 under an applied pressure of 1.8 GPa. Notably, the evaluated superconducting gaps in all these TMDs remain largely unaffected by changes in applied pressure, irrespective of pressure-induced partial suppression of CDW order in (4H/2H)-$NbSe_2$ or its general absence in 2H-NbS_2. These results underscore the complex nature of pressure-induced behaviors in these TMDs, challenging a simplistic view of competition solely between CDW order and superconductivity. Remarkably, the relationship between n_s/m^* and T_c exhibits an unconventional correlation, indicating a noteworthy similarity with the behavior observed in cuprate, kagome, and iron-based superconductors.

DOI: 10.1103/PhysRevResearch.7.013324

I. INTRODUCTION

Transition metal dichalcogenides (TMDs) [1,2] represent a fascinating class of materials that have garnered significant attention in condensed-matter physics due to their diverse electronic properties [3,4]. The superconducting state in TMDs has revealed an intriguing non-BCS behavior and unconventional superconducting states, in both bulk and monolayer form [5–8]. In particular, a correlation between the superfluid density and the transition temperature (T_c) serves as a notable manifestation of unconventional superconductivity in bulk 2H-$NbSe_2$ [1]. Additionally, the reported upper critical field (H_{c2}) values for 4H-$NbSe_2$ $\mu_0 H_{c2}(0) = 26.5$ T [9] and 2H-NbS_2 [$\mu_0 H_{c2}(0)\|_{ab} = 23$ T] [10] are much higher than the Pauli paramagnetic limit [$\mu_0 H_p = 1.84 \times T_c$ (T/K)] expected for a weakly coupled BCS superconductor. Recent advancements in the bulk TMD research have uncovered interesting phenomena, such as the observation of a Fulde-Ferrell-Larkin-Ovchinnikov state for magnetic fields applied exactly parallel to the *ab* plane [10,11]. The Ising-type superconductivity of monolayer 2H-$NbSe_2$ is, among other exceptional electronic properties, of particular interest [7]. These discoveries challenge conventional paradigms and open up new avenues for exploring unconventional superconductivity in TMDs, thereby expanding our understanding of the complex interplay between various electronic phases.

Furthermore, TMDs like 2H-$NbSe_2$ [12] and 4H-$NbSe_2$ [9] exhibit charge density wave (CDW) order in addition to superconductivity. The coexistence and interaction of these two phenomena raise intriguing questions about their origin, stability, and mutual influence. Pressure-induced phase transitions, which can suppress CDW order and alter superconducting behavior, offer valuable insights into the underlying mechanisms governing these phenomena [13–17]. Therefore, understanding the response of TMDs under pressure provides crucial information about the delicate balance between the competing electronic phases and sheds light on the unconventional nature of their superconducting state.

Building upon previous research [1,2], where a strong pressure effect on superfluid density and a correlation between

*These authors contributed equally to this work.
†Contact author: fabian.vonrohr@unige.ch
‡Contact author: zurab.guguchia@psi.ch

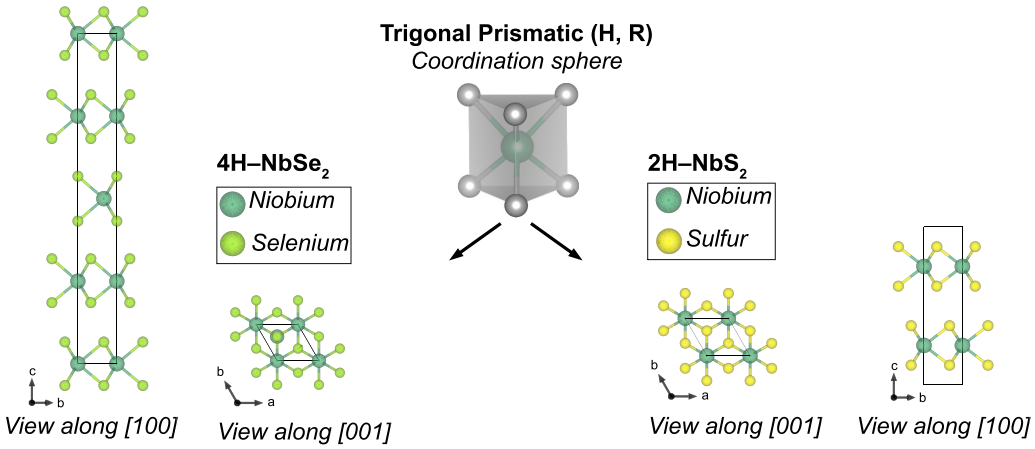

FIG. 1. Crystal structure. Middle: Illustration of the trigonal prismatic coordination sphere of the chalcogen atoms (yellow, sulfur; light green, selenium) around the niobium (dark green). Left: Side and top view of the 4H-$NbSe_2$, with four layers per unit cell. Right: Top and side view of the 2H-NbS_2, with two layers per unit cell [18].

superfluid density and T_c were demonstrated in 2H-$NbSe_2$, there is a pressing need to extend such investigations to encompass other members of the TMD family. Therefore, by systematically probing the superfluid density across different TMDs with and without CDW order we may unravel underlying trends and uncover the interplay between CDW order and superconductivity.

II. EXPERIMENTAL DETAILS AND RESULTS

In this article, we explore the hydrostatic pressure effects on the superfluid density (n_s/m^*) in both 4H-$NbSe_2$ and 2H-NbS_2, where the former exhibits CDW order, whereas the latter does not, while also comparing our findings to 2H-$NbSe_2$ with CDW order [1]. Figure 1 illustrates the crystal structure of the two studied systems. The 4H and 2H phases of these TMDs differ primarily in their stacking sequences and symmetry. Both phases have the same monolayer. While the 2H phase exhibits a hexagonal structure with AB stacking, the 4H phase features a more complex hexagonal structure with alternating stacking (ABAC). We observed a 75% increase in n_s/m^* in 4H-$NbSe_2$ at 2 GPa, while the onset temperature of the CDW order is reduced by only 20% (from 55 to 45 K). Notably, this increase in superfluid density in 4H-$NbSe_2$ is twice as large as that observed in 2H-$NbSe_2$, despite both systems experiencing a similar suppression of CDW order. Additionally, 2H-NbS_2 also exhibits a 20% increase in n_s/m^*. Regarding T_c, it increases by 1 K in 4H-$NbSe_2$, 0.5 K in 2H-$NbSe_2$, and 0.2 K in 2H-NbS_2. Therefore, 4H-$NbSe_2$ possesses the highest pressure effect on both n_s/m^* and T_c among the three systems studied. Furthermore, we demonstrate an unconventional correlation between n_s/m^* and T_c. These findings are discussed in the context of pressure-induced modifications of electron-phonon coupling, *p-d* hybridization, and density of states related to a saddle point situated very close to the Fermi level.

First, we present the impact of pressure on superconductivity and charge density wave order in 4H-$NbSe_2$ using magnetotransport measurements. Magnetotransport techniques [19–25], known for their sensitivity to charge-order transitions, leverage magnetoresistance as a probe of the mean free path integrated over the Fermi surface [22]. These techniques are particularly effective in detecting changes in scattering anisotropy and Fermi surface reconstructions. The CDW transition is evident in the Hall effect, as previously observed in 2H-$NbSe_2$ [23]. Figure 2(a) illustrates the temperature dependence of the longitudinal resistance measured under varying hydrostatic pressures up to 2.1 GPa. Sharp superconducting transitions are observed, with T_c showing a modest increase from 6.3 K at 0 GPa to 7.3 K at 2.1 GPa. Regarding the normal state, we find that the Hall effect exhibits a pronounced temperature dependence below $T_{CDW} = 55$ K in 4H-$NbSe_2$, at ambient pressure, indicating the onset of a CDW. Notably, the Hall signal transitions smoothly from negative (electronlike) to positive (holelike) across T^*. This sign reversal parallels observations in 2H-$NbSe_2$ [23] and cuprate high-temperature superconductors [24,25], where it has been attributed to Fermi-surface reconstruction driven by a density-wave phase. Similarly, in 4H-$NbSe_2$, the emergence of a secondary CDW order appears to induce a Fermi-surface reconstruction, resulting in the formation of the hole pocket. Additionally, magnetoresistance in 4H-$NbSe_2$ increases below $T_{CDW} = 55$ K at ambient pressure, further corroborating the onset of the CDW transition. The charge density wave transition is also observed as a very weak anomaly in the temperature dependence of longitudinal resistivity, appearing around 45 K. However, magnetoresistance and Hall effect measurements provide more compelling evidence for the onset of the CDW. Under applied pressure, both T_{CDW} and T^* exhibit only modest decrease, as summarized in Fig. 2(d). For comparison, the pressure dependence of T_{CDW} in 2H-$NbSe_2$ is also shown, highlighting a similar suppression of the CDW transition in both compounds. Within 2.1 GPa, the CDW transition temperature decreases by approximately 20%, while the superconducting transition temperature increases by 15%.

Next, we focus on superfluid density measurements for both 4H-$NbSe_2$ and 2H-NbS_2 under pressure by examining the superconducting (SC) relaxation rate (σ_{sc}) in the vortex state. The temperature (T) dependence of (σ_{sc}) is obtained by analyzing (see the Supplemental Material (SM) [26] for

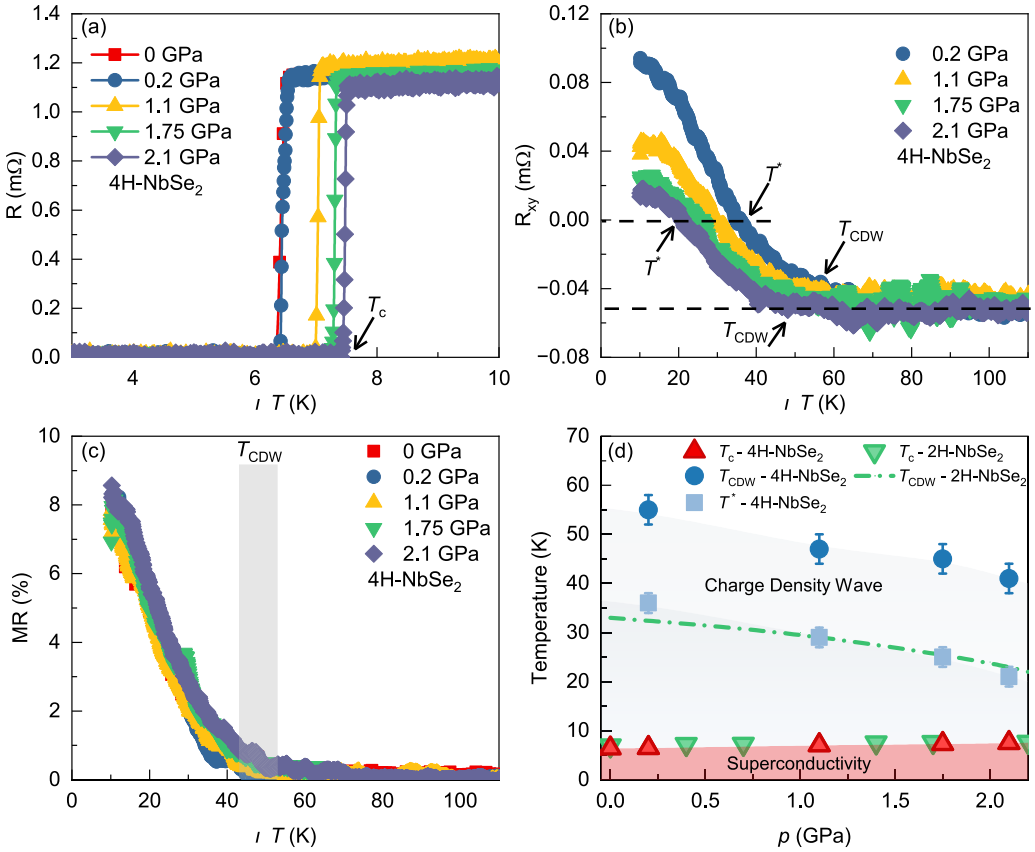

FIG. 2. Temperature-pressure phase diagram for 4H-$NbSe_2$. (a)–(c) The temperature dependence of (a) the longitudinal resistance, (b) the Hall resistance, and (c) the magnetoresistance at 9 T for 4H-$NbSe_2$, recorded under various hydrostatic pressures. (d) The pressure evolution of the superconducting transition temperature T_c, the onset of the CDW transition temperature T_{CDW}, and the temperature T^* across which the Hall effect changes the sign for 4H-$NbSe_2$, obtained from the resistivity measurements. For comparison, the values of T_c and T_{CDW} vs pressure for 2H-$NbSe_2$ are also shown [1].

details) the transverse field muon spin rotation (TF-μSR) data measured under an applied magnetic field of $\mu_0 H \simeq 30$ mT at ambient pressure (p) for both 4H-$NbSe_2$ and 2H-NbS_2 and are shown in the left y axis of Fig. 3(a). Below T_c, $\sigma_{sc}(T)$ for both systems gradually increases from zero due to the formation of the flux line lattice in the SC state and levels off at low temperatures ($T \leqslant 2$ K). Figure 3(b) shows the T dependence of the diamagnetic shifts, $\Delta B_{dia} = B_{int,s,sc} - B_{int,s,ns}$, for both systems. Here, $B_{int,s,sc}$ and $B_{int,s,ns}$ are the local internal fields experienced by the muons at superconducting and normal states of the sample, respectively. $B_{int,s,sc}$ is calculated from the first moment $\langle B \rangle$ of the asymmetric field distribution $P(B)$ in the superconducting state (see the SM [26]). As it can be seen from Fig. 3(b), such a strong diamagnetic shift below T_c reflects the bulk nature of the superconducting state and rules out any possibility of field-induced magnetism in both systems.

The effective (powder average) London magnetic penetration depths (λ_{eff}) are extracted for both systems from their corresponding σ_{sc} by using the relation $\sigma_{sc}(T)/\gamma_\mu = 0.06091\Phi_0 \times \lambda_{eff}^{-2}(T)$ [27]. Here, γ_μ is the gyromagnetic ratio of the muon, and $\Phi_0 = 2.068 \times 10^{-15}$ Wb is the magnetic-flux quantum. λ_{eff} is crucial to understanding superconductivity as it is a concomitant of superfluid density (n_s/m^*):

$$\sigma_{sc} \propto \frac{1}{\lambda_{eff}^2} = \frac{4\pi n_s e^2}{m^* c^2} \frac{1}{1 + \xi/l}, \tag{1}$$

where m^* is the effective mass of superconducting carriers, and ξ and l are the coherence length and mean free path, respectively. In the case of systems close to the clean limit ($\xi/l \to 0$), λ_{eff}^{-2} is directly proportional to the superfluid density, and $\lambda_{eff}^{-2} \propto n_s/m^*$ as the second term in Eq. (1) essentially becomes unity. By using the Ginzburg-Landau theory ($\xi = \sqrt{\Phi_0/2\pi H_{c2}}$) and reported upper critical field (H_{c2}) values for 4H-$NbSe_2$ [$\mu_0 H_{c2}(0) = 26.5$ T] [9] and for 2H-NbS_2 [$\mu_0 H_{c2}(0)\|_{ab} = 23$ T] [10], we have estimated the coherence lengths to be $\xi \simeq 3.5$ nm and $\xi\|_{ab} \simeq 3.8$ nm for 4H-$NbSe_2$ and 2H-NbS_2, respectively, at ambient pressure. Although an accurate estimate for l as a function of pressure is not available, it is reasonable to assume that the effect of ξ/l is negligible given the extremely small ξ. Moreover, the in-plane l is likely independent of pressure, as compression primarily affects the interlayer spacing rather than the intralayer structure, owing to the pronounced anisotropy of the van der Waals system. This is particularly relevant in the low-pressure range under investigation. Thus we can reliably take σ_{sc} and/or λ_{eff}^{-2}

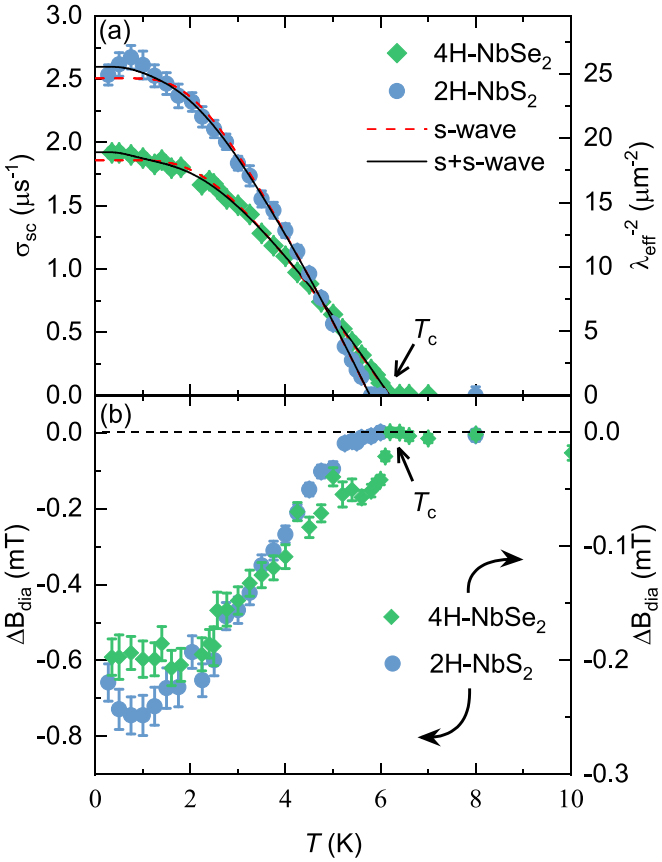

FIG. 3. Temperature evolution of microscopic superconducting quantities. (a) Temperature dependence of σ_{sc} (left y axis) and λ_{eff}^{-2} (right y axis) measured at an applied field of $\mu_0 H \simeq 30$ mT for both 4H-$NbSe_2$ and 2H-NbS_2. The black solid lines are the fits corresponding to the $(s+s)$-wave model, whereas the red dashed lines correspond to s-wave model fits. (b) Temperature dependence of ΔB_{dia} calculated from the difference between the internal fields measured at the superconducting and normal states for both systems.

as a measure of superfluid density ($\sigma_{sc} \propto \lambda_{eff}^{-2} \propto n_s/m^*$) as both systems lie close to the clean limit. To give a quantitative idea of n_s/m^*, we show λ_{eff}^{-2} in the right y axis of Fig. 3(a).

$\sigma_{sc}(T)$ is sensitive to the topology of the superconducting gap. In our case, the observed low-T leveling off behavior is consistent with the scenario of nodeless superconductivity, for which $\lambda_{eff}^{-2}(T)$ approaches the zero-T value exponentially. To unveil the nature of the superconducting gap structure in 4H-$NbSe_2$ and 2H-NbS_2, the T-dependent behavior of σ_{sc} for both compounds is analyzed by the empirical α model [4] within the local (London) approximation ($\lambda \gg \xi$). The main assumption of this model is that the gaps appearing in different bands are independent from one another, despite having a common T_c. So, the superfluid densities for each component can be calculated (for details, see the SM [26]) independently and added together with their respective weight factors as shown below:

$$\frac{\sigma_{sc}(T)}{\sigma_{sc}(0)} = \omega \frac{\sigma_{sc}(T, \Delta_{0,1})}{\sigma_{sc}(0, \Delta_{0,1})} + (1-\omega)\frac{\sigma_{sc}(T, \Delta_{0,2})}{\sigma_{sc}(0, \Delta_{0,2})}. \quad (2)$$

$\sigma_{sc}(0) \propto \lambda_{eff}^{-2}(0)$ and $\lambda_{eff}(0)$ is the magnetic penetration depth at $T = 0$ K. $\Delta_{0,i}$ measures the value of the ith ($i = 1$ and 2) SC gap at $T = 0$ K, whilst ω and $(1-\omega)$ are the weight factors quantifying their relative contributions to σ_{sc}. The results of our analysis are shown in Fig. 3(a), in which a single s-wave (red dashed line) model and a $(s+s)$-wave (black solid line) model are considered. It is clearly evident that a two gap $(s+s)$-wave model describes our data much better than a single gap s-wave model. Two-gap superconductivity in both systems can be understood by assuming that the SC gaps open at two distinct types of bands crossing the Fermi level (E_F). The values of superconducting gaps Δ_1 and Δ_2 (see the SM [26] for the pressure evolution of the SC gaps) are in good agreement with previous reports [1,9,28].

In order to study the pressure evolution of the superconducting order parameters of 4H-$NbSe_2$ and 2H-NbS_2, TF-μSR experiments are carried out under a pressure range of $0 \leqslant p \leqslant 2$ GPa. The TF-μSR time spectra recorded at different hydrostatic pressures are analyzed by adopting the procedure described in the SM [26]. To highlight the relative change of the superfluid density with pressure, we present the extracted T dependence of σ_{sc} at various applied pressures after normalizing each one to the value obtained at zero pressure and temperature for 4H-$NbSe_2$ and 2H-NbS_2 in Figs. 4(a) and 4(b), respectively. The two-gap $(s+s)$-wave model adequately describes all the experimental data up to the highest applied pressures with nearly pressure independent weight factors of $\omega \sim 0.54$ and 0.52 for 4H-$NbSe_2$ and 2H-NbS_2, respectively. The corresponding fits are shown by the black solid lines in Figs. 4(a) and 4(b). The absolute values of the two superconducting gaps (Δ_1 and Δ_2) extracted from the $(s+s)$-wave model fits remain almost constant throughout the applied pressure range for both systems, as depicted in Fig. S3 of the SM [26]. The pressure evolution of the other extracted superconducting parameters such as $\lambda_{eff}^{-2}(0)[\propto n_s/m^*]$ and T_c are plotted in Figs. 4(c) and 4(d), respectively, along with the corresponding pressure-dependent behavior of 2H-$NbSe_2$ for comparison, taken from our recent report (see Ref. [1]). As it is evident from Fig. 4(c), the relative increase of n_s/m^* with pressure for 4H-$NbSe_2$ is found to be the highest and corresponds to a 75% increase at the maximum applied pressure of 2.05 GPa. The relative increase is of 32% for 2H-$NbSe_2$ and only 20% for 2H-NbS_2, at the maximum applied pressures of 2.2 and 1.8 GPa, respectively. However, the critical temperatures T_c of all systems are found to be notably less influenced by the increase of pressure. T_c increases by 0.94 K (16%) for 4H-$NbSe_2$, 0.76 K (11%) for 2H-$NbSe_2$, and 0.28 K (5%) for 2H-NbS_2.

III. DISCUSSION

The primary discovery of this study lies in the remarkable increase of superfluid density (n_s/m^*) under pressure, particularly in 4H-$NbSe_2$, surpassing its counterparts 2H-$NbSe_2$ and 2H-NbS_2. The p-T phase diagram of 2H-$NbSe_2$, which has been thoroughly explored in the past [13–15], indicates a linear rise in T_c with pressure, alongside a systematic suppression of the CDW order (T_{CDW}). Here, we have constructed the temperature-pressure phase diagram for 4H-$NbSe_2$ using magnetotransport measurements, revealing a similar increase

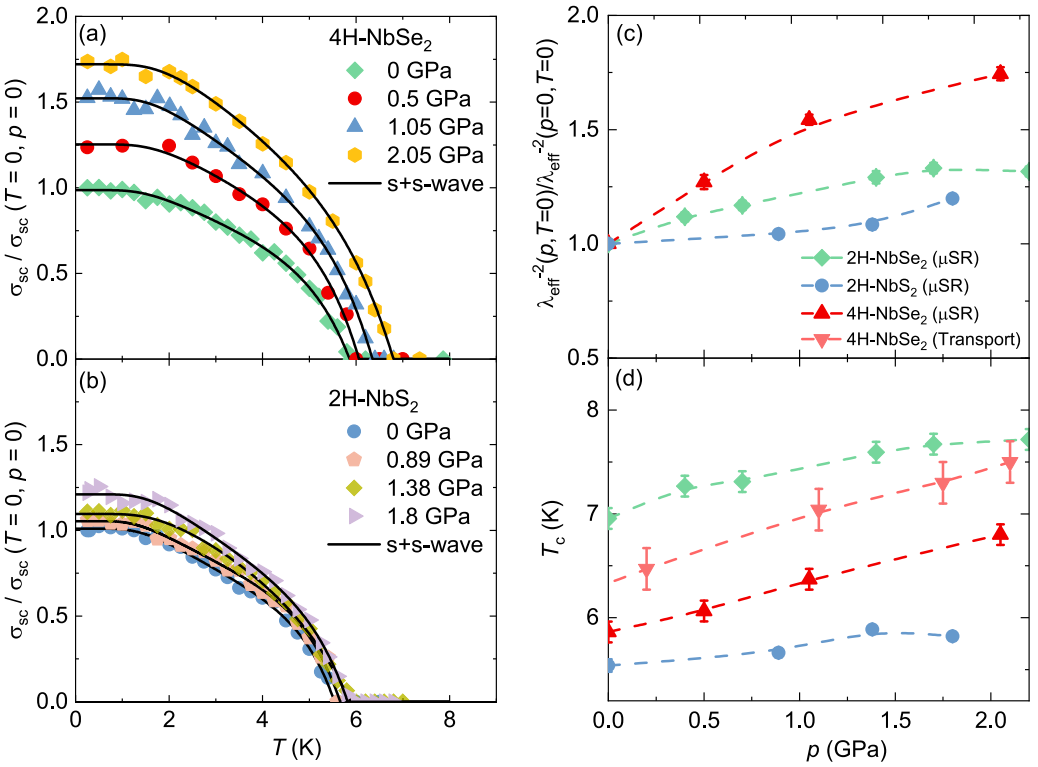

FIG. 4. Temperature and pressure evolution of superconducting quantities. The temperature dependence of $\sigma_{sc}(T)$ (normalized to the value at zero applied pressure) under different applied hydrostatic pressures for (a) 4H-$NbSe_2$ and (b) 2H-NbS_2, respectively. The solid lines are the fits corresponding to the $(s + s)$-wave model. Pressure dependence of (c) normalized zero temperature value of $\lambda_{eff}^{-2}(0)$ and (d) T_c. The values of T_c for 4H-$NbSe_2$, determined from both resistivity and μSR experiments, are shown.

in T_c and a comparable suppression of the CDW onset temperature as observed in 2H-$NbSe_2$. The antagonistic pressure dependence of T_c and T_{CDW} sparked the notion of mutual competition between CDW order and superconductivity, which continues to be an ongoing debate [16,17]. However, despite the absence of a CDW state in all known NbS_2 polytypes, the T_c of 2H-NbS_2 is comparable to that of 4H-$NbSe_2$, albeit with a higher superfluid density. Additionally, the modest suppression of the CDW state within the 2.1-GPa pressure range for 2H-$NbSe_2$, and 4H-$NbSe_2$, suggests that the substantial increase in superfluid density cannot solely stem from the CDW state suppression, especially considering the maximal availability of the density of states, $\Delta D(E_F) \approx 1\%$ [29,30]. Remarkably, a 20% increase in the superfluid density is also observed for 2H-NbS_2, which is devoid of the CDW order present in the other TMDs, (4H/2H)-$NbSe_2$. The insensitivity of the two superconducting gaps (Δ_1, Δ_2) to pressure changes across all investigated TMDs, (4H/2H)-$NbSe_2$ with a CDW and 2H-NbS_2 [31–33] without a CDW, suggests a more complex origin for the significant pressure effects beyond the competing CDW order.

In 2H-$NbSe_2$, the Fermi surface (FS) structure is intricate, featuring predominantly four Nb ($4d$)-orbital-derived bands forming cylindrical Fermi surface sheets centered around the mid-Γ and corner-K points, along with one Se ($4p$)-orbital-derived band resembling a small three-dimensional "pancake" FS centered around the Γ point. Superconductivity manifests through the opening of two gaps: a relatively large gap spanning most of the Nb-derived FS sheets and a smaller one at the Se-derived band. Meanwhile, a coexisting CDW opens a gap on a small portion of the Nb-derived FS sheets, distinct from the superconducting gaps in k-space [34–36]. There is a growing evidence that the CDW order in 2H-$NbSe_2$ is primarily driven by momentum (q)-dependent electron-phonon coupling (EPC) rather than the previous belief of mechanisms involving Fermi-surface nesting and saddle points, etc. [30,37–39]. Furthermore, recent *ab initio* band structure calculations on 4H-$NbSe_2$ [9] propose that the lower T_c and higher T_{CDW} could be linked to weaker p-d hybridization and the availability of additional density of states near the Fermi level compared to 2H-$NbSe_2$. Consequently, a pressure-dependent complex interplay among various factors such as EPC, multiband FS structure, and p-d hybridization likely underlies the substantial pressure-induced change in superfluid density observed in 4H-$NbSe_2$ [14,40].

The strong increase in superfluid density in TMDs underscores their unconventional superconductivity, contrasting with the behavior observed in conventional BCS superconductors. This is supported by the correlation between T_c and zero-T values of the superfluid densities [$\lambda_{eff}^{-2}(0)$] observed in 4H-$NbSe_2$ and 2H-NbS_2, as well as previously reported materials such as 2H-$NbSe_2$ [1] and 1T′-$MoTe_2$ [2]. The plotted data in Fig. 5, illustrating the relative change in T_c as a function of the relative change in superfluid density [41], shows that the slopes for 2H-$NbSe_2$, 4H-$NbSe_2$, and 2H-NbS_2 are the same, suggesting a similar mechanism for the pressure-induced enhancement of the superfluid density. Intriguingly, this slope resembles that observed in optimally

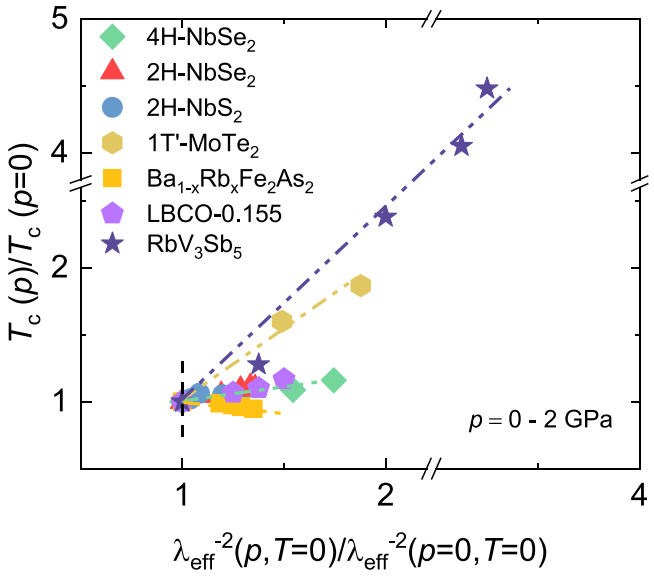

FIG. 5. Superconducting critical temperature versus superfluid density. Plot of $T_c(p)/T_c(p=0)$ vs normalized superfluid density at different applied pressures obtained from our μSR experiments in 4H-$NbSe_2$, 2H-$NbSe_2$ [1], 2H-NbS_2, 1T′-$MoTe_2$ [2], $Ba_{1-x}Rb_xFe_2As_2$ [43], $La_{2-x}Ba_xCuO_4$ ($x = 0.155$) [42], and RbV_3Sb_5 [50]. The black dashed vertical line manifests the BCS expectation.

doped cuprates [42] and Fe-based superconductors [43], although the sign of the slope is opposite in Fe-based systems. Conversely, 1T′-$MoTe_2$ and RbV_3Sb_5 exhibit a stronger slope, despite their T_c remaining below the optimal value even under pressure [2,44,50]. In contrast, 4H-NbSe2, 2H-$NbSe_2$ [1], and 2H-NbS_2 are closer to their optimal $T_c \simeq 8$ K [45].

The observed correlation between T_c and the superfluid density, initially observed in cuprates [46] and later extended to Fe-based unconventional superconductors [47–49] and kagome-lattice superconductors [50], reveals intriguing insights [41]. In cuprates, T_c is about 4–5 times lower than the expected ideal Bose condensation temperature (T_B) for a noninteracting Bose gas, indicating an evolution from an unconventional Bose-Einstein condensation (BEC)-like scenario to a conventional BCS-type condensation scenario [51–53]. In the investigated TMDs, the ratio T_c/T_F is reduced by approximately 20 times compared to cuprates, yet the unconventional correlation persists. This striking similarity across distinct classes of superconductors implies a shared mechanism underlying superconductivity and other quantum orders in these materials. The variation in the slope of the T_c-superfluid density correlation across systems remains unclear. Two key factors likely influence T_c in unconventional superconductors: superfluid density and proximity to a competing state or quantum critical point. In cuprates, this competing state is tied to antiferromagnetic order, while in Fe-based superconductors it is linked to quantum criticality. In TMD and kagome-lattice systems, the competing state arises from CDW or structural orders. These differences in competing states may explain the varying slopes in the T_c-superfluid density correlation.

IV. CONCLUSION

In conclusion, we investigated the effects of hydrostatic pressure on the microscopic properties of superconductivity in 4H-$NbSe_2$ and 2H-NbS_2, alongside the pressure evolution of the CDW in 4H-$NbSe_2$ using magnetotransport and μSR experiments. We find that the CDW onset temperature in 4H-$NbSe_2$ decreases by only 20% (from 55 to 45 K), similar to 2H-$NbSe_2$. Despite similar CDW suppression in 2H- and 4H-$NbSe_2$, the superfluid density increase is twice as strong in 4H-$NbSe_2$. Additionally, a sizable increase in superfluid density is observed in 2H-NbS_2, which lacks CDW order. These findings lead us to infer that the increase in the superfluid density and the underlying superconductivity in these systems are minimally impacted by pressure-induced changes in the CDW order. Instead, they may have a more complex origin, possibly involving additional factors beyond the influence of the CDW order. Notably, an unconventional correlation between T_c and n_s/m^* is evident across all the studied TMDs, including the previously investigated topological superconductor 1T′-$MoTe_2$, reflecting a characteristic feature of unconventional superconductors, such as cuprates and Fe-based superconductors. We anticipate that our study will inspire future theoretical investigations, such as band structure calculations under pressure, as well as experimental investigations (e.g., angle-resolved photoemission spectroscopy), to achieve a comprehensive understanding of superconductivity in these TMDs, particularly in 4H-$NbSe_2$.

ACKNOWLEDGMENTS

The μSR experiments were carried out at the Swiss Muon Source (SμS), Paul Scherrer Institute, Villigen, Switzerland. This work was supported by the Swiss National Science Foundation (SNSF) through SNSF Starting Grant No. TMSGI2_211750.

Z.G. conceived and designed the project. Z.G. and F.O.v.R. supervised the project. Other duties were carried as follows: crystal growth, C.W. and F.v.R.; high-pressure magnetotransport experiments and analysis, V.S. and Z.G. with contributions from S.S.I., O.G., P.K., and M.B.; muon spin rotation experiments under pressure and corresponding analysis, Z.G., S.S.I., J.N.G., H.L., and R.K.; and figure development and writing of the paper, Z.G. and S.S.I. with contributions from all authors. All authors discussed the results, interpretation, and conclusion.

[1] F. O. von Rohr, J.-C. Orain, R. Khasanov, C. Witteveen, Z. Shermadini, A. Nikitin, J. Chang, A. R. Wieteska, A. N. Pasupathy, M. Z. Hasan, A. Amato, H. Luetkens, Y. J. Uemura, and Z. Guguchia, Unconventional scaling of the superfluid density with the critical temperature in transition metal dichalcogenides, Sci. Adv. **5**, eaav8465 (2019).

[2] Z. Guguchia, F. von Rohr, Z. Shermadini, A. T. Lee, S. Banerjee, A. R. Wieteska, C. A. Marianetti, B. A. Frandsen,

H. Luetkens, Z. Gong, S. C. Cheung, C. Baines, A. Shengelaya, G. Taniashvili, A. N. Pasupathy, E. Morenzoni, S. J. L. Billinge, A. Amato, R. J. Cava, R. Khasanov *et al.*, Signatures of the topological s^{+-} superconducting order parameter in the type-II Weyl semimetal T_d-$MoTe_2$, Nat. Commun. **8**, 1082 (2017).

[3] Q. H. Wang, A. Bedoya-Pinto, M. Blei, A. H. Dismukes, A. Hamo, S. Jenkins, M. Koperski, Y. Liu, Q.-C. Sun, E. J. Telford, H. H. Kim, M. Augustin, U. Vool, J.-X. Yin, L. H. Li, A. Falin, C. R. Dean, F. Casanova, R. F. L. Evans, M. Chshiev *et al.*, The magnetic genome of two-dimensional van der Waals materials, ACS Nano **16**, 6960 (2022).

[4] Z. Guguchia, A. Kerelsky, D. Edelberg, S. Banerjee, F. von Rohr, D. Scullion, M. Augustin, M. Scully, D. A. Rhodes, Z. Shermadini, H. Luetkens, A. Shengelaya, C. Baines, E. Morenzoni, A. Amato, J. C. Hone, R. Khasanov, S. J. L. Billinge, E. Santos, A. N. Pasupathy *et al.*, Magnetism in semiconducting molybdenum dichalcogenides, Sci. Adv. **4**, eaat3672 (2018).

[5] B. Sipos, A. F. Kusmartseva, A. Akrap, H. Berger, L. Forró, and E. Tutiš, From Mott state to superconductivity in 1T-TaS_2, Nat. Mater. **7**, 960 (2008).

[6] A. Ribak, R. M. Skiff, M. Mograbi, P. K. Rout, M. H. Fischer, J. Ruhman, K. Chashka, Y. Dagan, and A. Kanigel, Chiral superconductivity in the alternate stacking compound 4Hb-TaS_2, Sci. Adv. **6**, eaax9480 (2020).

[7] X. Xi, Z. Wang, W. Zhao, J.-H. Park, K. T. Law, H. Berger, L. Forró, J. Shan, and K. F. Mak, Ising pairing in superconducting $NbSe_2$ atomic layers, Nat. Phys. **12**, 139 (2016).

[8] H. Zhang, A. Rousuli, K. Zhang, L. Luo, C. Guo, X. Cong, Z. Lin, C. Bao, H. Zhang, S. Xu, R. Feng, S. Shen, K. Zhao, W. Yao, Y. Wu, S. Ji, X. Chen, P. Tan, Q.-K. Xue, Y. Xu *et al.*, Tailored Ising superconductivity in intercalated bulk $NbSe_2$, Nat. Phys. **18**, 1425 (2022).

[9] M. Zhou, Y. Gu, S. Ni, B. Ruan, Q. Liu, Q. Yang, L. Chen, J. Yi, Y. Shi, G. Chen, and Z. Ren, Structures, charge density wave, and superconductivity of noncentrosymmetric $4H_a$-$NbSe_2$, Phys. Rev. B **108**, 224518 (2023).

[10] C.-w. Cho, J. Lyu, C. Y. Ng, J. J. He, K. T. Lo, D. Chareev, T. A. Abdel-Baset, M. Abdel-Hafiez, and R. Lortz, Evidence for the Fulde–Ferrell–Larkin–Ovchinnikov state in bulk NbS_2, Nat. Commun. **12**, 3676 (2021).

[11] P. Wan, O. Zheliuk, N. F. Q. Yuan, X. Peng, L. Zhang, M. Liang, U. Zeitler, S. Wiedmann, N. E. Hussey, T. T. M. Palstra, and J. Ye, Orbital Fulde–Ferrell–Larkin–Ovchinnikov state in an Ising superconductor, Nature (London) **619**, 46 (2023).

[12] S. Yoshizawa, K. Sagisaka, and H. Sakata, Visualization of alternating triangular domains of charge density waves in $2H$-$NbSe_2$ by scanning tunneling microscopy, Phys. Rev. Lett. **132**, 056401 (2024).

[13] C. Berthier, P. Molinié, and D. Jérome, Evidence for a connection between charge density waves and the pressure enhancement of superconductivity in $2H$-$NbSe_2$, Solid State Commun. **18**, 1393 (1976).

[14] H. Suderow, V. G. Tissen, J. P. Brison, J. L. Martínez, and S. Vieira, Pressure induced effects on the Fermi surface of superconducting $2H$-$NbSe_2$, Phys. Rev. Lett. **95**, 117006 (2005).

[15] Y. Feng, J. Wang, R. Jaramillo, J. van Wezel, S. Haravifard, G. Srajer, Y. Liu, Z.-A. Xu, P. B. Littlewood, and T. F. Rosenbaum, Order parameter fluctuations at a buried quantum critical point, Proc. Natl. Acad. Sci. USA **109**, 7224 (2012).

[16] O. Moulding, I. Osmond, F. Flicker, T. Muramatsu, and S. Friedemann, Absence of superconducting dome at the charge-density-wave quantum phase transition in $2H$-$NbSe_2$, Phys. Rev. Res. **2**, 043392 (2020).

[17] Z.-Y. Cao, K. Zhang, A. F. Goncharov, X.-J. Yang, Z.-A. Xu, and X.-J. Chen, Pressure effect of the charge density wave transition on raman spectra and transport properties of $2H$-$NbSe_2$, Phys. Rev. B **107**, 245125 (2023).

[18] K. Momma and F. Izumi, *VESTA3* for three-dimensional visualization of crystal, volumetric and morphology data, J. Appl. Crystallogr. **44**, 1272 (2011).

[19] P. Giraldo-Gallo, J. A. Galvis, Z. Stegen, K. A. Modic, F. F. Balakirev, J. B. Betts, X. Lian, C. Moir, S. C. Riggs, J. Wu, A. T. Bollinger, X. He, I. Božović, B. J. Ramshaw, R. D. McDonald, G. S. Boebinger, and A. Shekhter, Scale-invariant magnetoresistance in a cuprate superconductor, Science **361**, 479 (2018).

[20] M. Novak, S. Sasaki, K. Segawa, and Y. Ando, Large linear magnetoresistance in the Dirac semimetal TlBiSSe, Phys. Rev. B **91**, 041203(R) (2015).

[21] X. Wei, C. Tian, H. Cui, Y. Li, S. Liu, Y. Feng, J. Cui, Y. Song, Z. Wang, and J.-H. Chen, Linear nonsaturating magnetoresistance in kagome superconductor CsV_3Sb_5 thin flakes, 2D Mater. **10**, 015010 (2023).

[22] L. Das, Y. Xu, T. Shang, A. Steppke, M. Horio, J. Choi, S. Jöhr, K. von Arx, J. Mueller, D. Biscette, X. Zhang, A. Schilling, V. Granata, R. Fittipaldi, A. Vecchione, and J. Chang, Two-carrier magnetoresistance: Applications to $Ca_3Ru_2O_7$, J. Phys. Soc. Jpn. **90**, 054702 (2021).

[23] L. Li, J. Shen, Z. Xu, and H. Wang, Magnetoresistance and Hall effect of two-dimensional $2H$-$NbSe_2$, Int. J. Mod. Phys. B **19**, 275 (2005).

[24] D. LeBoeuf, N. Doiron-Leyraud, J. Levallois, R. Daou, J.-B. Bonnemaison, N. E. Hussey, L. Balicas, B. J. Ramshaw, R. Liang, D. A. Bonn, W. N. Hardy, S. Adachi, C. Proust, and L. Taillefer, Electron pockets in the Fermi surface of hole-doped high-T_c superconductors, Nature (London) **450**, 533 (2007).

[25] D. LeBoeuf, N. Doiron-Leyraud, B. Vignolle, M. Sutherland, B. J. Ramshaw, J. Levallois, R. Daou, F. Laliberté, O. Cyr-Choinière, J. Chang, Y. J. Jo, L. Balicas, R. Liang, D. A. Bonn, W. N. Hardy, C. Proust, and L. Taillefer, Lifshitz critical point in the cuprate superconductor $YBa_2Cu_3O_y$ from high-field Hall effect measurements, Phys. Rev. B **83**, 054506 (2011).

[26] See Supplemental Material at http://link.aps.org/supplemental/10.1103/PhysRevResearch.7.013324 for details related to x-ray diffraction, and μSR experiments, as well as the fitting procedures and parameters, which includes Ref. [43,54–60].

[27] E. H. Brandt, Properties of the ideal Ginzburg-Landau vortex lattice, Phys. Rev. B **68**, 054506 (2003).

[28] P. Diener, M. Leroux, L. Cario, T. Klein, and P. Rodière, In-plane magnetic penetration depth in NbS_2, Phys. Rev. B **84**, 054531 (2011).

[29] K. Rossnagel, O. Seifarth, L. Kipp, M. Skibowski, D. Voß, P. Krüger, A. Mazur, and J. Pollmann, Fermi surface of $2H$-$NbSe_2$ and its implications on the charge-density-wave mechanism, Phys. Rev. B **64**, 235119 (2001).

[30] M. D. Johannes, I. I. Mazin, and C. A. Howells, Fermi-surface nesting and the origin of the charge-density wave in $NbSe_2$, Phys. Rev. B **73**, 205102 (2006).

[31] V. G. Tissen, M. R. Osorio, J. P. Brison, N. M. Nemes, M. García-Hernández, L. Cario, P. Rodière, S. Vieira, and H. Suderow, Pressure dependence of superconducting critical temperature and upper critical field of $2H$-NbS_2, Phys. Rev. B **87**, 134502 (2013).

[32] C. Heil, S. Poncé, H. Lambert, M. Schlipf, E. R. Margine, and F. Giustino, Origin of superconductivity and latent charge density wave in NbS_2, Phys. Rev. Lett. **119**, 087003 (2017).

[33] Z. El Youbi, S. W. Jung, C. Richter, K. Hricovini, C. Cacho, and M. D. Watson, Fermiology and electron-phonon coupling in the $2H$ and $3R$ polytypes of NbS_2, Phys. Rev. B **103**, 155105 (2021).

[34] T. Yokoya, T. Kiss, A. Chainani, S. Shin, M. Nohara, and H. Takagi, Fermi surface sheet-dependent superconductivity in $2H$-$NbSe_2$, Science **294**, 2518 (2001).

[35] S. V. Borisenko, A. A. Kordyuk, V. B. Zabolotnyy, D. S. Inosov, D. Evtushinsky, B. Büchner, A. N. Yaresko, A. Varykhalov, R. Follath, W. Eberhardt, L. Patthey, and H. Berger, Two energy gaps and Fermi-surface "arcs" in $NbSe_2$, Phys. Rev. Lett. **102**, 166402 (2009).

[36] D. J. Rahn, S. Hellmann, M. Kalläne, C. Sohrt, T. K. Kim, L. Kipp, and K. Rossnagel, Gaps and kinks in the electronic structure of the superconductor $2H$-$NbSe_2$ from angle-resolved photoemission at 1 K, Phys. Rev. B **85**, 224532 (2012).

[37] M. D. Johannes and I. I. Mazin, Fermi surface nesting and the origin of charge density waves in metals, Phys. Rev. B **77**, 165135 (2008).

[38] F. Weber, S. Rosenkranz, J.-P. Castellan, R. Osborn, R. Hott, R. Heid, K.-P. Bohnen, T. Egami, A. H. Said, and D. Reznik, Extended phonon collapse and the origin of the charge-density wave in $2H$-$NbSe_2$, Phys. Rev. Lett. **107**, 107403 (2011).

[39] T. Valla, A. V. Fedorov, P. D. Johnson, P.-A. Glans, C. McGuinness, K. E. Smith, E. Y. Andrei, and H. Berger, Quasiparticle spectra, charge-density waves, superconductivity, and electron-phonon coupling in $2H$-$NbSe_2$, Phys. Rev. Lett. **92**, 086401 (2004).

[40] M. Leroux, I. Errea, M. Le Tacon, S.-M. Souliou, G. Garbarino, L. Cario, A. Bosak, F. Mauri, M. Calandra, and P. Rodière, Strong anharmonicity induces quantum melting of charge density wave in $2H$-$NbSe_2$ under pressure, Phys. Rev. B **92**, 140303(R) (2015).

[41] D. Das, R. Gupta, C. Baines, H. Luetkens, D. Kaczorowski, Z. Guguchia, and R. Khasanov, Unconventional pressure dependence of the superfluid density in the nodeless topological superconductor α-$PdBi_2$, Phys. Rev. Lett. **127**, 217002 (2021).

[42] Z. Guguchia, R. Khasanov, A. Shengelaya, E. Pomjakushina, S. J. L. Billinge, A. Amato, E. Morenzoni, and H. Keller, Cooperative coupling of static magnetism and bulk superconductivity in the stripe phase of $La_{2-x}Ba_xCuO_4$: Pressure- and doping-dependent studies, Phys. Rev. B **94**, 214511 (2016).

[43] Z. Guguchia, A. Amato, J. Kang, H. Luetkens, P. K. Biswas, G. Prando, F. von Rohr, Z. Bukowski, A. Shengelaya, H. Keller, E. Morenzoni, R. M. Fernandes, and R. Khasanov, Direct evidence for a pressure-induced nodal superconducting gap in the $Ba_{0.65}Rb_{0.35}Fe_2As_2$ superconductor, Nat. Commun. **6**, 8863 (2015).

[44] Y. Qi, P. G. Naumov, M. N. Ali, C. R. Rajamathi, W. Schnelle, O. Barkalov, M. Hanfland, S.-C. Wu, C. Shekhar, Y. Sun, V. Süß, M. Schmidt, U. Schwarz, E. Pippel, P. Werner, R. Hillebrand, T. Förster, E. Kampert, S. Parkin, R. J. Cava *et al.*, Superconductivity in Weyl semimetal candidate $MoTe_2$, Nat. Commun. **7**, 11038 (2016).

[45] A. Majumdar, D. VanGennep, J. Brisbois, D. Chareev, A. V. Sadakov, A. S. Usoltsev, M. Mito, A. V. Silhanek, T. Sarkar, A. Hassan, O. Karis, R. Ahuja, and M. Abdel-Hafiez, Interplay of charge density wave and multiband superconductivity in layered quasi-two-dimensional materials: The case of $2H$-NbS_2 and $2H$-$NbSe_2$, Phys. Rev. Mater. **4**, 084005 (2020).

[46] Y. J. Uemura, G. M. Luke, B. J. Sternlieb, J. H. Brewer, J. F. Carolan, W. N. Hardy, R. Kadono, J. R. Kempton, R. F. Kiefl, S. R. Kreitzman, P. Mulhern, T. M. Riseman, D. L. Williams, B. X. Yang, S. Uchida, H. Takagi, J. Gopalakrishnan, A. W. Sleight, M. A. Subramanian, C. L. Chien *et al.*, Universal correlations between T_c and $\frac{n_s}{m^*}$ (carrier density over effective mass) in high-T_c cuprate superconductors, Phys. Rev. Lett. **62**, 2317 (1989).

[47] H. Luetkens, H.-H. Klauss, M. Kraken, F. J. Litterst, T. Dellmann, R. Klingeler, C. Hess, R. Khasanov, A. Amato, C. Baines, M. Kosmala, O. J. Schumann, M. Braden, J. Hamann-Borrero, N. Leps, A. Kondrat, G. Behr, J. Werner, and B. Büchner, The electronic phase diagram of the $LaO_{1-x}F_xFeAs$ superconductor, Nat. Mater. **8**, 305 (2009).

[48] R. Khasanov, H. Luetkens, A. Amato, H.-H. Klauss, Z.-A. Ren, J. Yang, W. Lu, and Z.-X. Zhao, Muon spin rotation studies of $SmFeAsO_{0.85}$ and $NdFeAsO_{0.85}$ superconductors, Phys. Rev. B **78**, 092506 (2008).

[49] H. Luetkens, H.-H. Klauss, R. Khasanov, A. Amato, R. Klingeler, I. Hellmann, N. Leps, A. Kondrat, C. Hess, A. Köhler, G. Behr, J. Werner, and B. Büchner, Field and temperature dependence of the superfluid density in $LaFeAsO_{1-x}F_x$ superconductors: A muon spin relaxation study, Phys. Rev. Lett. **101**, 097009 (2008).

[50] Z. Guguchia, R. Khasanov, and H. Luetkens, Unconventional charge order and superconductivity in kagome-lattice systems as seen by muon-spin rotation, npj Quantum Mater. **8**, 41 (2023).

[51] Y. J. Uemura, L. P. Le, G. M. Luke, B. J. Sternlieb, W. D. Wu, J. H. Brewer, T. M. Riseman, C. L. Seaman, M. B. Maple, M. Ishikawa, D. G. Hinks, J. D. Jorgensen, G. Saito, and H. Yamochi, Basic similarities among cuprate, bismuthate, organic, Chevrel-phase, and heavy-fermion superconductors shown by penetration-depth measurements, Phys. Rev. Lett. **66**, 2665 (1991).

[52] Y. J. Uemura, A. Keren, L. P. Le, G. M. Luke, B. J. Sternlieb, W. D. Wu, J. H. Brewer, R. L. Whetten, S. M. Huang, S. Lin, R. B. Kaner, F. Diederich, S. Donovan, G. Grüner, and K. Holczer, Magnetic-field penetration depth in K_3C_{60} measured by muon spin relaxation, Nature (London) **352**, 605 (1991).

[53] Y. J. Uemura, Condensation, excitation, pairing, and superfluid density in high-T_c superconductors: the magnetic resonance mode as a roton analogue and a possible spin-mediated pairing, J. Phys.: Condens. Matter **16**, S4515 (2004).

[54] F. Jellinek, G. Brauer, and H. Müller, Molybdenum and niobium sulphides, Nature (London) **185**, 376 (1960).

[55] B. E. Brown and D. J. Beerntsen, Layer structure polytypism among niobium and tantalum selenides, Acta Cryst. **18**, 31 (1965).

[56] R. Khasanov, D. G. Eshchenko, D. Di Castro, A. Shengelaya, F. La Mattina, A. Maisuradze, C. Baines, H. Luetkens, J. Karpinski, S. M. Kazakov, and H. Keller, Magnetic penetration depth in RbOs2O6 studied by muon spin rotation, Phys. Rev. B **72**, 104504 (2005).

[57] A. Maisuradze, A. Shengelaya, A. Amato, E. Pomjakushina, and H. Keller, Muon spin rotation investigation of the pressure effect on the magnetic penetration depth in $YBa_2Cu_3O_x$, Phys. Rev. B **84**, 184523 (2011).

[58] A. Suter and B. Wojek, Musrfit: A free platform-independent framework for SR data analysis, Phys. Procedia **30**, 69 (2012).

[59] M. Tinkham, *Introduction to Superconductivity*, 2nd ed. (Dover Publications, Mineola, New York, 2004).

[60] A. Carrington and F. Manzano, Magnetic penetration depth of MgB_2, Physica C: Superconductivity **385**, 205 (2003).